Design of an Edge-Coupled Dual-Ring Split-Ring Resonator

Anju Pradeep, S. Mridula, and P. Mohanan

Division of Electronics Engineering, School of Engineering
Cochin University of Science and Technology, Kochi, Kerala, India, Pin-682022
Tel: 091484-2862349 (AP, SM); 091484-2862339 (PM)
E-mail: anjupradeep@cusat.ac.in; mridula@cusat.ac.in; drmohan@ieee.org

Abstract

Electric permittivity and magnetic permeability control electromagnetic wave propagation through materials. In naturally occurring materials, these are positive. Artificial materials exhibiting negative material properties have been reported: they are referred to as metamaterials. This paper concentrates on a ring-type split-ring resonator (SRR) exhibiting negative magnetic permeability. The design and synthesis of the SRR using the genetic-algorithm approach is explained in detail. A user-friendly graphical user interface (GUI) for an SRR optimizer and estimator using *MATLAB*™ is also presented.

Keywords: Edge coupled SRR; genetic algorithm; metamaterials; permeability; perturbation method

1. Introduction

In 1897, H. G.W ells portrayed a scientist changing the refractive index of his body so that his body did not absorb or reflect light, and he became invisible. Today, scientists are capable of constructing devices that can "cloak" objects [1]. These artificial materials (metamaterials) have the ability to bend electromagnetic waves around the object so that the object becomes invisible. (The prefix "meta" means "beyond" in Greek). Metamaterials are a new class of ordered composites that exhibit exceptional properties not readily observed in nature. These properties arise from qualitatively new response functions. These properties (1) are not observed in the constituent materials, and (2) they result from the inclusion of artificially fabricated, low-dimensional inhomogeneities. In electromagnetism, metamaterials gain their properties from their structure, rather than directly from their composition. Materials with such exotic properties have the potential to radically change the worlds of wireless, optical communication, radar, and surveillance. Their unique characteristics can result in antenna miniaturization. In addition, the technology may enable the creation of miniaturized RF lenses with a unique sub-wavelength resolution capability, as well as ultra-fast signaling between two points. At optical frequencies, metamaterial super-resolving lenses could enable printing microelectronic devices with light at nanoscales.

A material medium consisting of metallic inclusions randomly or periodically distributed inside a host dielectric behaves – at least, within a range of frequencies – as an effective continuous medium the electromagnetic constitutive parameters of which have values well outside the range of ordinary materials [2]. Most popular metamaterials are sub-wavelength thin wires (for negative permittivity) and split-ring resonators (for negative permeability). When the electric field (E) is parallel to the wires and the magnetic field (H) is perpendicular to the plane of the rings, electric and magnetic dipoles are generated in the wires and rings, respectively. This leads to polarization, which results in metamaterial properties.

Most commonly used metamaterials are based on the use of split-ring resonators (SRRs), originally proposed by Pendry et al. [3]. These consist of two concentric rings separated by a gap, both having splits on the opposite sides. An array of SRRs exhibits negative effective permeability for frequencies close to the magnetic resonance frequency. Magnetic resonance is induced by the splits at the rings, and by the gap between the inner and outer rings. The application of an axial, uniform, and time-varying magnetic field to the rings induces current loops at resonance. The open metal loop forms an *LC* oscillating circuit. These current loops are closed through the distributed capacitance between the concentric rings, and the system behaves as an *LC* resonator. Because of the current circulation between the rings and the relatively large value of capacitance achievable, the electric size of the particle can be made small at resonance.

Current loops can also be induced by a uniform time-varying electric field lying in the particle's plane, and oriented in the direction orthogonal to the imaginary line connecting the slits. This is due to the dipolar electric moment induced in the rings, as a consequence of the cross-polarization effects present in the SRR's first resonance. The magnetic response of the resulting artificial material can be expressed in terms of

continuous medium parameters, provided that the dimensions and the inter-element spacing between the individual resonators are small compared to the wavelength. This bianisotropic behavior of SRRs is closely related to their topology. On the basis of the above concepts, different SRR configurations exist in order to avoid or enhance some SRR properties.

The commonly used SRR configurations [4] are shown in Figure 1. EC-SRR stands for edge-coupled SRR, which is the conventional SRR. The broadside-coupled SRR (BC-SRR) was proposed to avoid cross-polarization effects, as well as to further reduce the electrical size of the SRR at resonance. The non-bianisotropic SRR (NB-SRR) is used to avoid cross-polarization effects while keeping the single-plane geometry of the SRR.

SRRs can be of different geometrical shapes. They can be circular or rectangular, as shown in Figure 2 [5].

An edge-coupled two-ring SRR was selected as the object of study in this paper. In principle, any excitation can be used to study the current distribution at SRR resonances. The

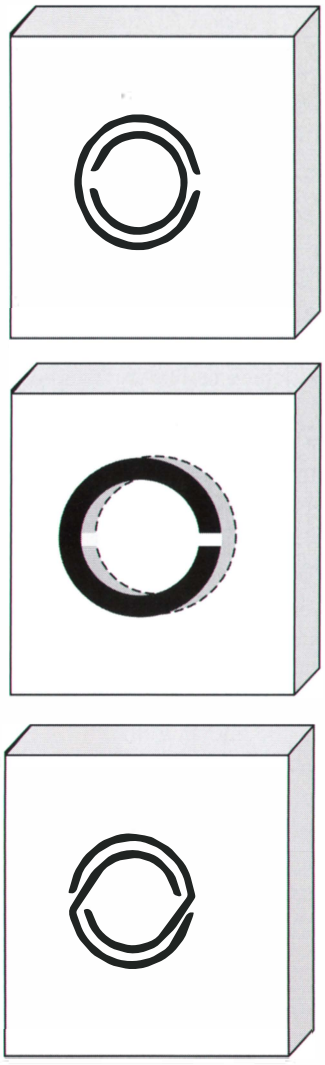

Figure 1. Common split-ring resonator (SRR) configurations: (a) Edge-coupled SRR (EC-SRR); (b) Broadside-coupled SRR (BC-SRR); (c) Non-bianisotropic SRR (NB-SRR).

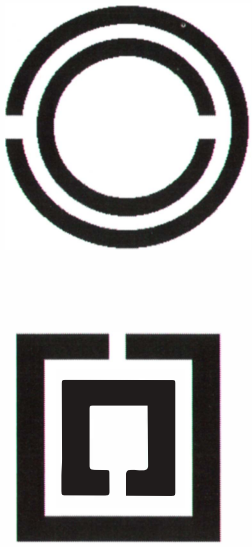

Figure 2. (a) A circular SRR; (b) A rectangular SRR.

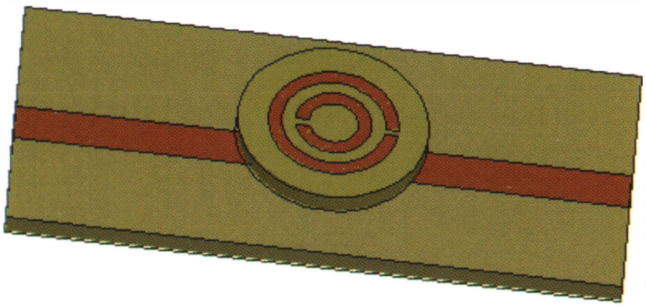

Figure 3. A SRR placed on a 50 Ω transmission line.

arrangement used for the present study to simulate SRR properties is shown in Figure 3. The SRR was placed on a 50 Ω microstrip transmission line, etched on a substrate. From the S_{21} characteristics, the resonant frequency of the SRR could be easily determined.

2. Evidence of Negative Permeability

Several theoretical explanations are available to justify the presence of and to evaluate the negative permeability of an SRR array [5]. In the search of evidence for negative permeability, a waveguide-cavity perturbation method is employed. Cavity-perturbation techniques are frequently used to measure the complex magnetic and dielectric properties of materials at microwave frequencies. Bethe and Schwinger first proposed the cavity-perturbation theory in 1943 [6]. In 1960, Waldron presented the detailed perturbation formula, with necessary approximations [7]. This technique is highly sensitive and accurate, and is therefore advantageous in the determination of permittivity and permeability. The technique is based on the change in the resonant frequency and quality factor of the cavity due to insertion of a sample inside the cavity at the position of the maximum in electric field and magnetic field, for the measurement of the permittivity and permeability, respectively [8, 9].

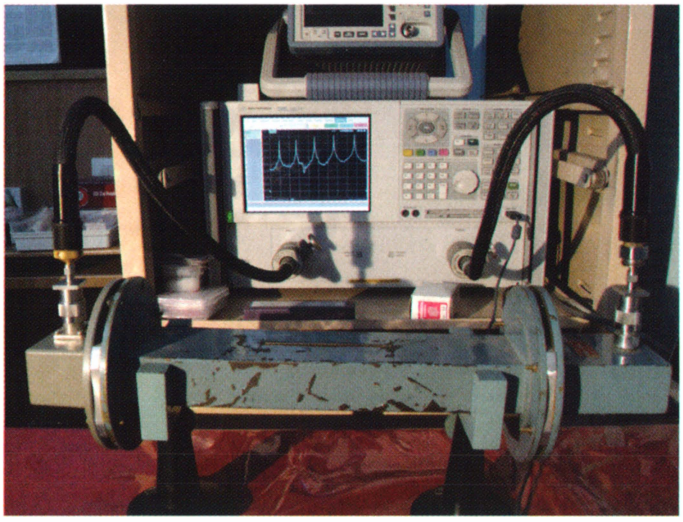

Figure 4. The experimental setup for cavity perturbation.

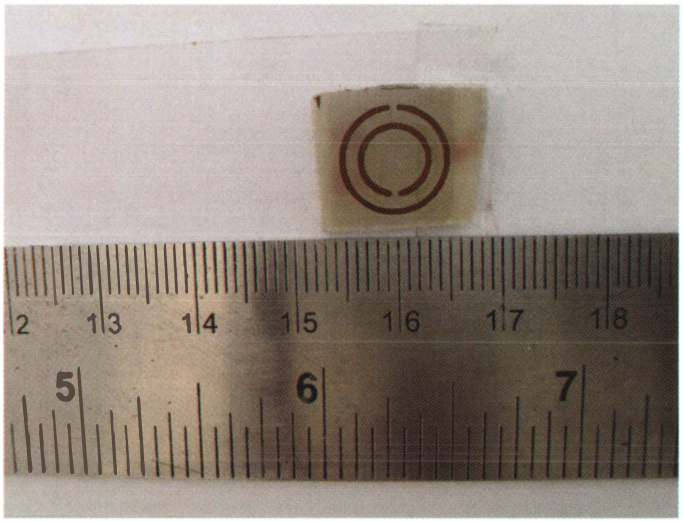

Figure 5. The SRR used for cavity perturbation.

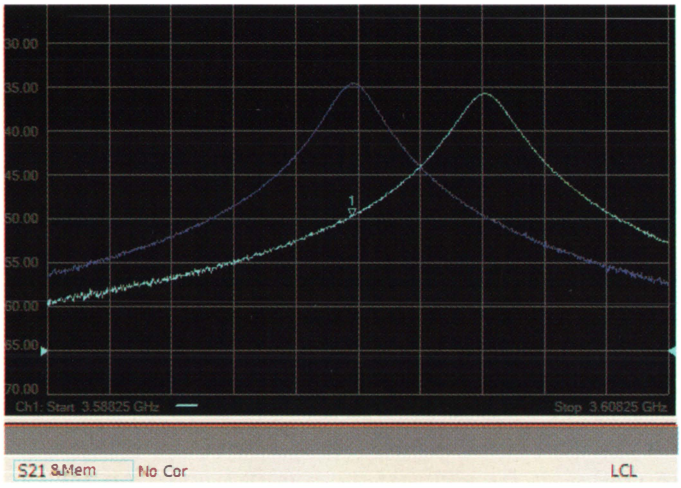

Figure 6. The resonant frequency of the cavity in the even mode at 3.59 GHz: (blue) without the SRR; (green) with the SRR.

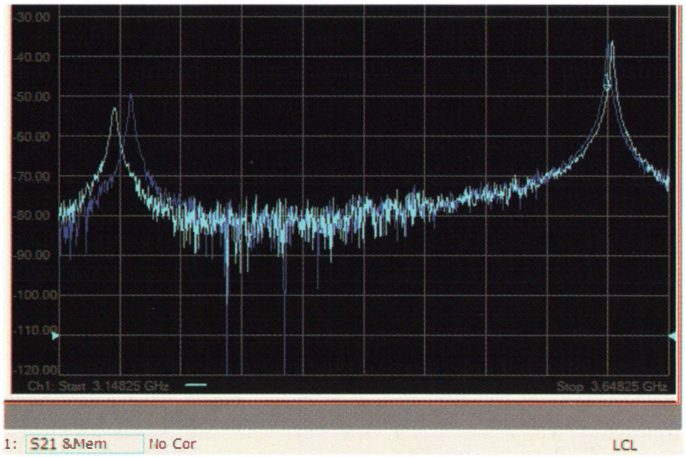

Figure 7. The resonant frequency of the cavity in the odd and even modes: (blue) without the SRR; (green) with the SRR.

The experimental setup for measuring permittivity and permeability is shown in Figure 4. The SRR was inserted into the narrow slotted-rectangular-waveguide cavity, at the position of maximum magnetic field for even TE_{10n} modes, where n is the longitudinal mode number. The SRR was aligned in such a way that the magnetic field was perpendicular to the slits in the SRR, to ensure maximum magnetic interaction with the SRR. A photograph of the SRR used for the experiment is shown in Figure 5.

Figure 6 shows the resonance behavior of the empty waveguide cavity (blue) and of the cavity loaded with the SRR (green) at the position of maximum magnetic field. An SRR of resonant frequency 2.55 GHz was used for measurement, and the first even mode after 2.55 GHz, which occurred at 3.59 GHz, is shown in figure as the reference. It is very interesting to note that when the SRR was at the maximum of the magnetic field (this happened exactly at the center of the cavity for even TE_{10n} modes, with n equal to an even integer), the shift in resonance frequency was towards the right. That meant that the resonance frequency was increased with the loading of the SRR. When the sample was at the middle of the waveguide cavity, the shift in the resonant frequency of the odd modes was towards the left, and that for the even modes was towards the right. This is shown in Figure 7. The left shift in resonant frequency for the odd mode was due to the positive permittivity of the substrate.

This indicated an increase in frequency with perturbation, which is possible only if the perturbing structure exhibits negative permeability, as per the well-known cavity-perturbation formula:

$$\mu = 1 + \left[\frac{(f_0 - f_s)}{f_s} \frac{v_c}{v_s} \right] K , \qquad (1)$$

where f_0 is the mode frequency of the empty cavity; f_s is the shifted frequency with the sample; v_c and v_s are the volumes of the cavity and the substrate, respectively; and K is a constant.

For the even mode, the shift in resonant frequency was small, due to the small polarizability of a single SRR. The important inference of this experiment was the presence of negative permeability, and that the shift occurred only for the cavity mode corresponding to the magnetic field, after the first resonant frequency of the SRR, when placed at the maximum of the magnetic field. No right shift was observed at the even mode of 3.59 GHz, when an SRR with a resonant frequency of 4.5 GHz was placed at the middle of the cavity.

To prove that the right shift occurred due to the negative permeability of the SRR, a positive-permeability material (nickel) was introduced into the cavity, and a shift in resonant frequency was observed. It was seen that the positive permeability produced a left shift in the even mode, as expected. This is shown in Figure 8.

It could thus be seen that an SRR produced a right shift of the resonant frequency within a cavity for the mode where magnetic field was maximum, and the shift occurred for the even mode after the resonant frequency of the SRR.

It is also well known that negative permeability is due to antisymmetric resonance. This was clearly evident from the current distributions shown in Figures 9a and 9b for the first and second resonances. It could be seen that the current direction was opposite at the splits for the first resonance, and in the same direction during the second resonance. This proved that negative permeability occurred in the immediate vicinity of the first resonance after the resonant frequency of the SRR.

The shift in resonance is a measure of the permeability, as specified by Equation (1). However, permeability itself seems to depend on various parameters of the SRR. Hence, quantifying the permeability calls for detailed study, which is not covered in this paper.

3. Development of Design Equation

The geometry of a dual-ring SRR, along with its parameters, are shown in Figure 10. The input impedance of the SRR

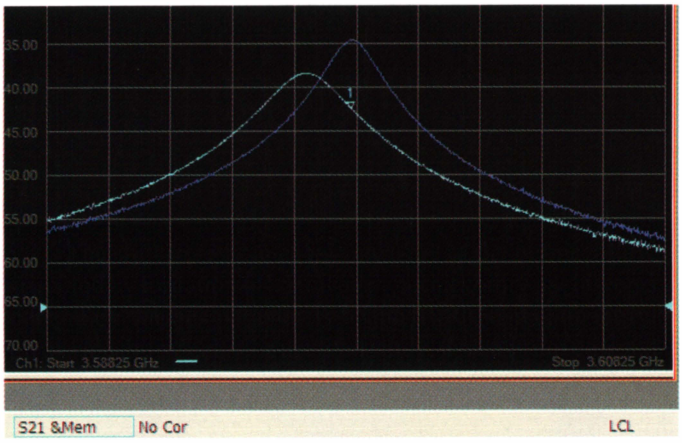

Figure 8. The resonant curve of the cavity for the even mode: (blue) the cavity alone; (green) the cavity with the nickel sample.

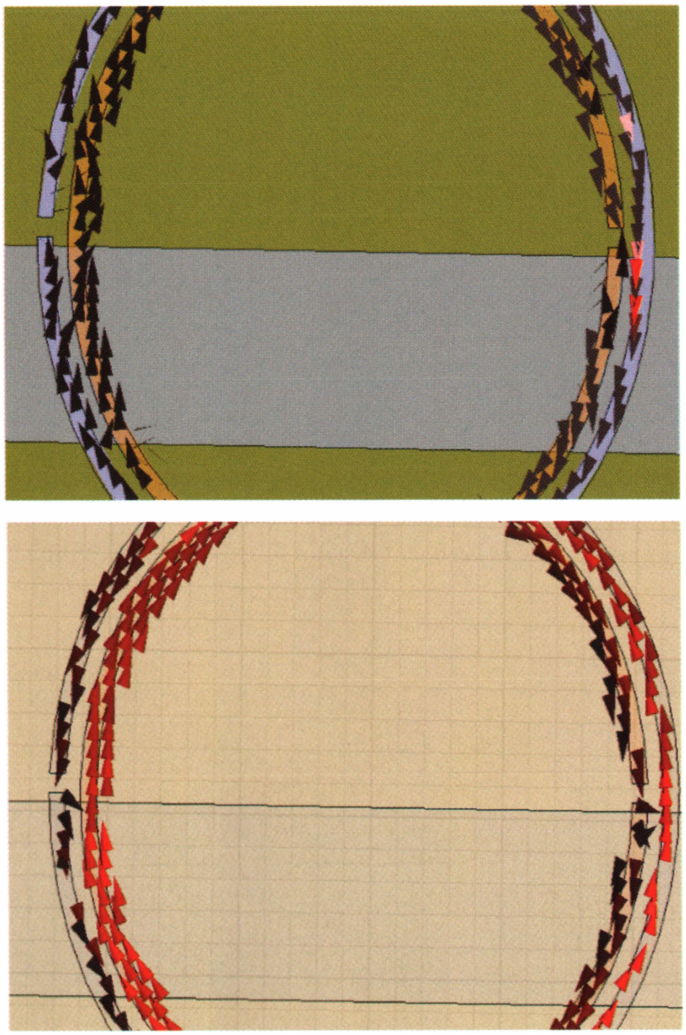

Figure 9. The current distribution in the SRR at resonance: (a) first resonance, (b) second resonance.

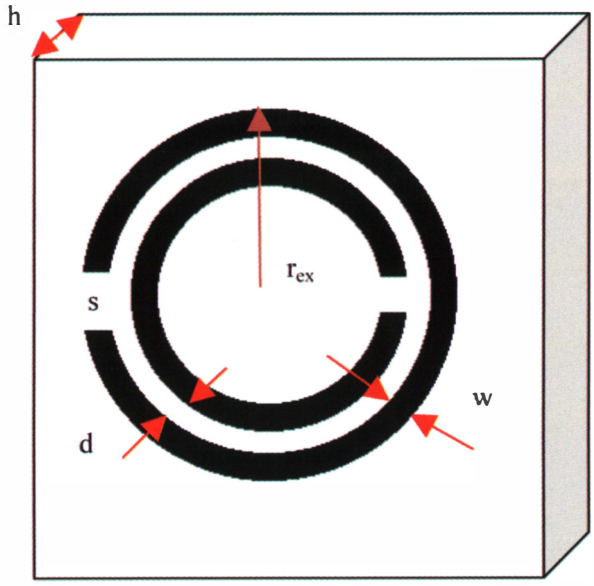

Figure 10. The dual-ring SRR. r_{ext} is the external radius (6 mm), w is the width of the ring (0.3 mm), d is the gap between rings (0.3 mm), s is the width of the slit in the ring (0.3 mm), h is the height of the substrate (1.6 mm), and ε_r is the relative permittivity of the substrate (4.4).

placed on a microstrip transmission line, as shown in Figure 3, was simulated in the range of 1-10 GHz using Ansoft's *HFSS*. Since the SRR can be considered to consist of lumped parameters at resonance [10], the reactance at the resonant frequency was noted from the Smith chart for different parameters of the SRR. The influence of different parameters is explained in the following paragraphs.

From experiment and simulation studies, it was found that the variation in reactance was virtually independent of the width of the slits(s). Hence, s was selected as 0.3 mm for the present study. The variations of the resonant frequency and the reactance with the various parameters of the SRR are shown in Figures 11a-11e.

The resonant frequency was found to increase with the width of the rings (w) and with the gap between the rings (d), as was evident from Figures 11a-11b. It was found that the reactance of the circuit was highly influenced by the SRR's parameters. The reactance variation showed both an inductive and a capacitive nature. As expected, the resonant frequency decreased with an increase in the radius of the outer ring (r_{ext}),

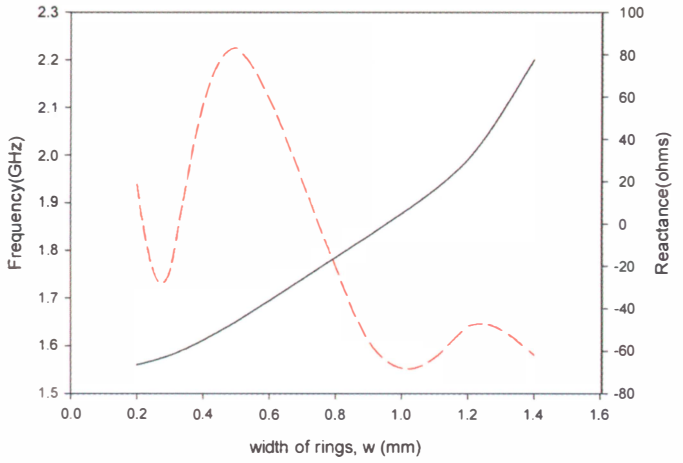

Figure 11a. The parametric variation of the resonant frequency (solid line) and reactance (dashed line) with a change in the width of the rings.

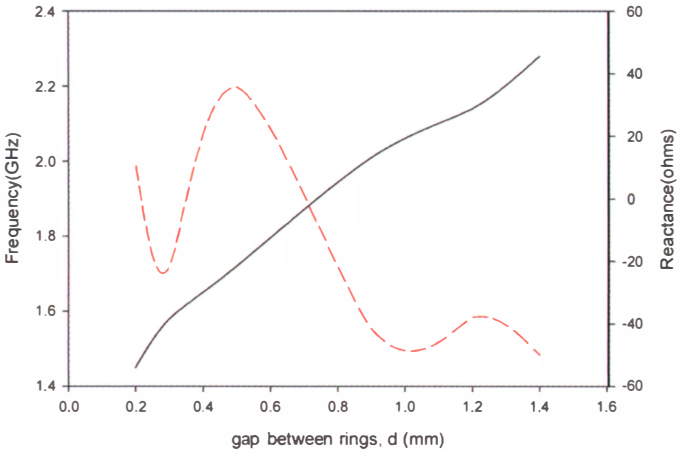

Figure 11b. The parametric variation of the resonant frequency (solid line) and reactance (dashed line) with the gap between the rings.

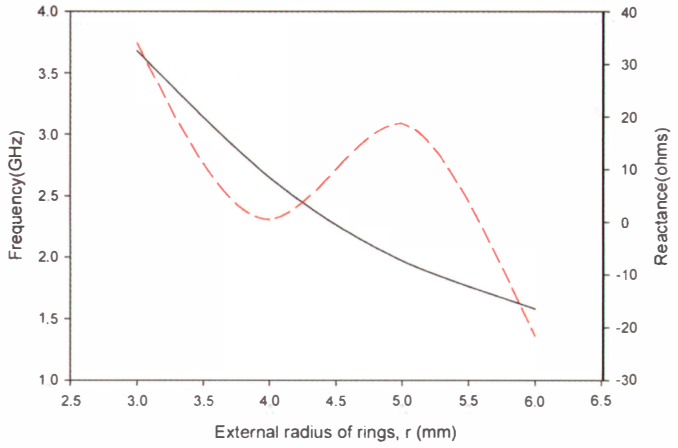

Figure 11c. The parametric variation of the resonant frequency (solid line) and reactance (dashed line) with the external radius of the rings.

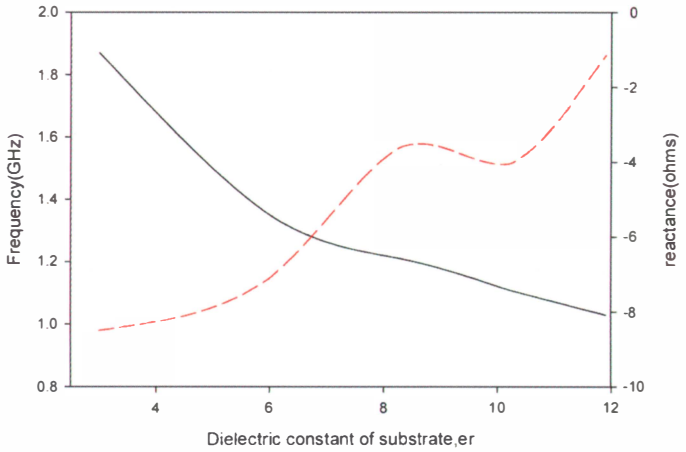

Figure 11d. The parametric variation of the resonant frequency (solid line) and reactance (dashed line) with the dielectric constant.

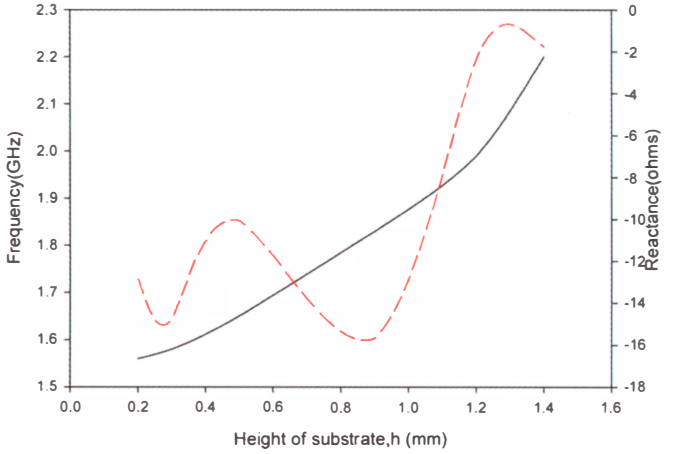

Figure 11e. The parametric variation of the resonant frequency (solid line) and reactance (dashed line) with the height of the substrate.

as shown in Figure 11c. The substrate's dielectric constant also influenced the resonance behavior of the SRR (Figure 11d). The resonant frequency increased with the substrate thickness (h) (Figure 11e).

To develop a design equation for the resonant frequency of the SRR, a 50 Ω microstrip transmission line of 3 mm width and 25 mm length was simulated in the frequency range of 0.5 GHz to 7 GHz using *IE3D*™. The parameter extraction was done, and the L and C values were stored as reference.

The SRR was then placed above the transmission line, and the simulation was repeated for different parametric values. The differences in the inductance and capacitance at the resonant frequency, with and without the SRR, were found. Using curve fitting, the inductance and capacitance of the SRR were numerically found, as follows:

$$L = 2.57e^{\frac{-w_3}{\sqrt{2}}}\left(\pi r_{ext} - 2.2d_1 - \frac{\pi}{2}\right), \quad (2)$$

$$\begin{aligned} C &= 0.217 \\ &+ \left\{\left[0.059\left(2r_{ext} + \varepsilon_r - 5\right)\right]\left(0.437w_1 - 0.317w_2^2 + 0.07w_2^3\right)\right. \\ &\left.\left(3.3367e^{-3.2d_1} - 0.1955e^{-0.47h}\right)\right\} \\ &+ \left(0.05\varepsilon_r - 0.218\right) + \left(\frac{0.599h}{0.0248 + h} - 0.599\right), \quad (3) \end{aligned}$$

where $w_1 = w$, $w_2 = 2$, $w_3 = w$ for $d < 1$ mm; $w_1 = w/3$, $w_2 = 1.414w$, $w_3 = w/1.414$ for $d > 1$ mm; $d_1 = d$ for $d < 1$ mm; and $d_1 = 1.414d$ for $d > 1$ mm. The correction factors for d and w were obtained after exhaustive experimental and simulation studies.

Once the lumped parameters were available, the resonant frequency for the SRR was calculated using the standard relationship:

$$F = \frac{1}{2\pi\sqrt{LC}} \text{ for } r > 5.2 \text{ mm}. \quad (4)$$

To incorporate the nonlinearity in parameters, a corrective term was added in order to minimize the error:

$$F = \frac{1}{2\pi\sqrt{LC}} + \frac{5.2 - r_{ext}}{2} \text{ for } r < 5.2 \text{ mm}. \quad (5)$$

The validity of this relationship was confirmed through experiment and simulation. A comparison of the resonant frequency obtained using Equations (4) and (5) and the simulation are shown graphically in Figures 12a-12e. The equation was verified for frequencies from 1 GHz to 8 GHz, and was found to hold well within a 10% error.

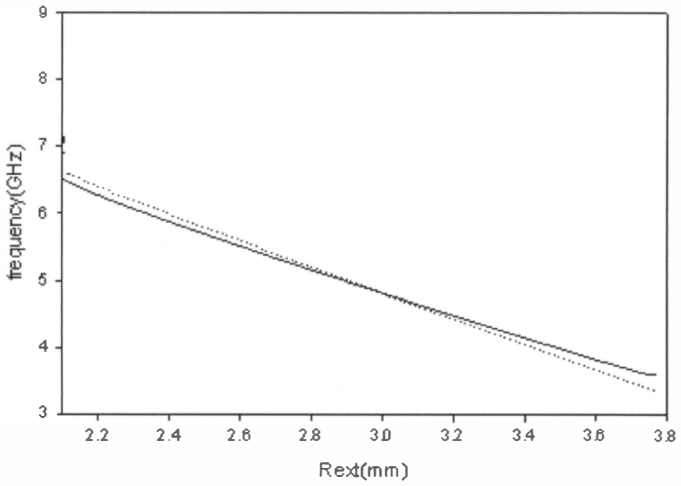

Figure 12a. Validation of the design equation: the resonant frequency as a function of the radius for the equation (solid line) and the simulation (dashed line).

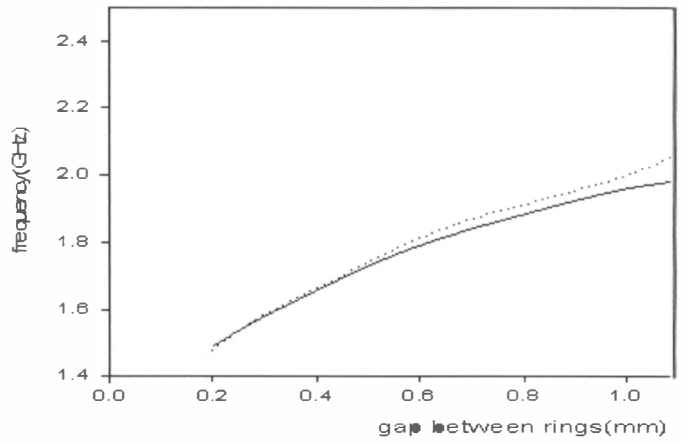

Figure 12b. Validation of the design equation: the resonant frequency as a function of the gap for the equation (solid line) and the simulation (dashed line).

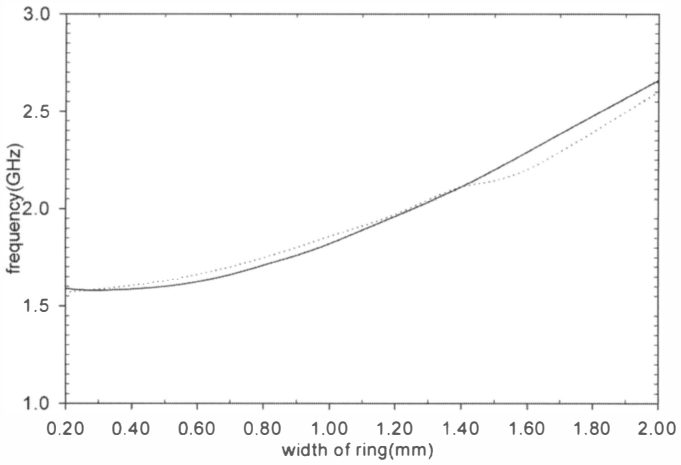

Figure 12c. Validation of the design equation: the resonant frequency as a function of the width for the equation (solid line) and the simulation (dashed line).

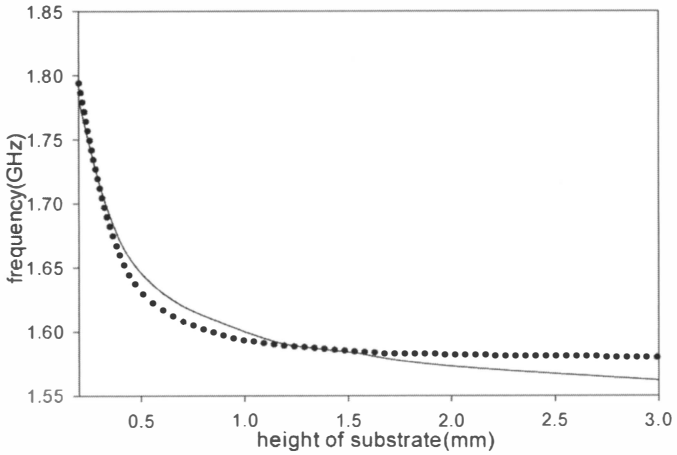

Figure 12d. Validation of the design equation: the resonant frequency as a function of the height of the substrate for the equation (solid line) and the simulation (dashed line).

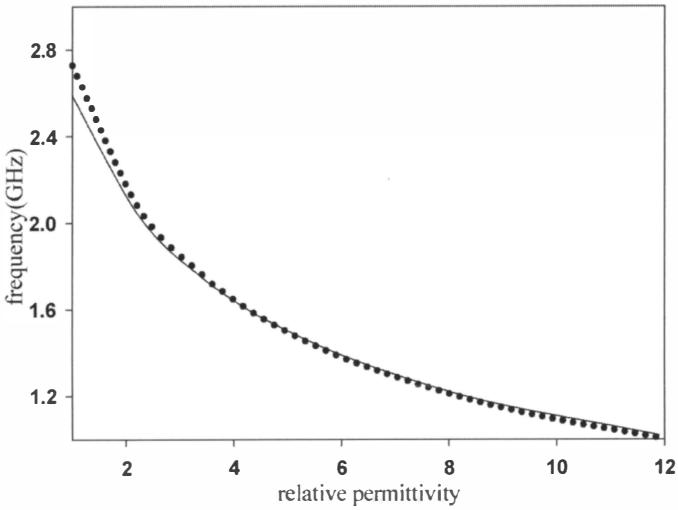

Figure 12e. Validation of the design equation: the resonant frequency as a function of the relative permittivity for the equation (solid line) and the simulation (dashed line).

4. A Genetic-Algorithm Optimizer for the SRR's Resonant Frequency

The genetic algorithm (GA) is a robust and global search algorithm that can be applied for optimization in any field of science [11-13]. When used appropriately, a genetic algorithm can yield satisfactory results while avoiding laborious mathematical calculations. For all problems that have a feasible solution, the genetic algorithm converges to the solution in a simple and elegant manner.

Genetic-algorithm optimizers are stochastic search methods modeled on the concepts of natural selection and evolution. Genetic-algorithm optimizers efficiently search for and locate global maxima in a near-optimal manner. The concept of the genetic algorithm was first formalized by John Holland (1975), and extended to functional optimization by De Jong (1975). The genetic algorithm involves the use of search strategies patterned after the Darwinian notion of natural selection and evolution. During a genetic-algorithm optimization, a set of trial solutions or population is chosen, and "evolves" toward an optimal solution under the "selective pressure" of the object function. The parameter set representing each trial solution or individual is coded to form a string or chromosome. Each individual is assigned a fitness value by evaluation of the objective function. The objective function is the only link between the genetic-algorithm optimizer and the physical problem. The coded parameters, represented by a set of 1s and 0s for binary coding. are called "genes." The first population is created randomly. The object function is calculated using each chromosome. The entire population is assigned a cost or fitness, based on the variation from the desired result. A few chromosomes from this population are selected as parents from this set, based on different selection techniques of the genetic algorithm. Some bits of the bit patterns that represent the genes of two parents are interchanged to perform crossing over, to get a new offspring. The set of new offspring thus obtained gives rise to the second generation. The second generation may or may not contain the parents. The cost evaluation and crossing over continues until an optimum result is achieved. To increase the diversity of the population, a small percentage of bit reversal or mutation is performed at random locations within a population in each generation.

A simple genetic algorithm must be able to perform five basic tasks: encode the solution parameters in the form of chromosomes, initialize a starting-point population, evaluate and assign fitness values to individuals in the population, perform reproduction through the fitness-weighted selection of individuals from the population, and perform recombination and mutation to produce members of the next generation.

4.1 The SRR Optimizer

When a SRR for a particular frequency is desired, the conventional approach requires a lengthy iteration process. In order to avoid such a time-consuming process, a genetic algorithm (GA) was used to develop an optimized software code to get the dimensions of the SRR.

The parameters used for developing the optimizer were the external radius of the SRR (r_{ext}), the width of the rings (w), and the gap between the rings (d). All of the dimensions were specified in millimeters. The split in the rings (s) was selected as 0.3 mm, as mentioned in Section 3. The substrate properties were treated as input parameters to be provided by the end user. A chromosome consisted of three genes: r_{ext} , w, and d. Four bits each were used for w and d, and six bits were used for the external radius (r_{ext}). To avoid the null condition of an all-zero-bit combination, the minimum values of w and d were fixed at 0.2 mm. For the external radius, the minimum was fixed at 1.7 mm and 3 mm for frequencies greater than 4 GHz and less than 4 GHz, respectively (since the size of the SRR is inversely proportional to the external radius). The first six bits of the chromosome represented the external radius, the next four bits represented the width of the rings, and the last four bits provided the gap between rings. Thus,

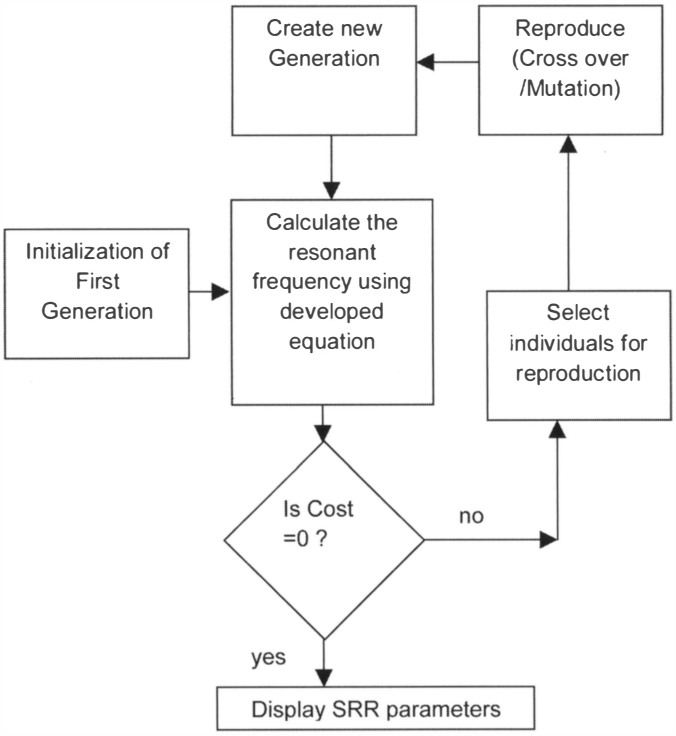

Figure 13. A flowchart of the genetic-algorithm optimizer.

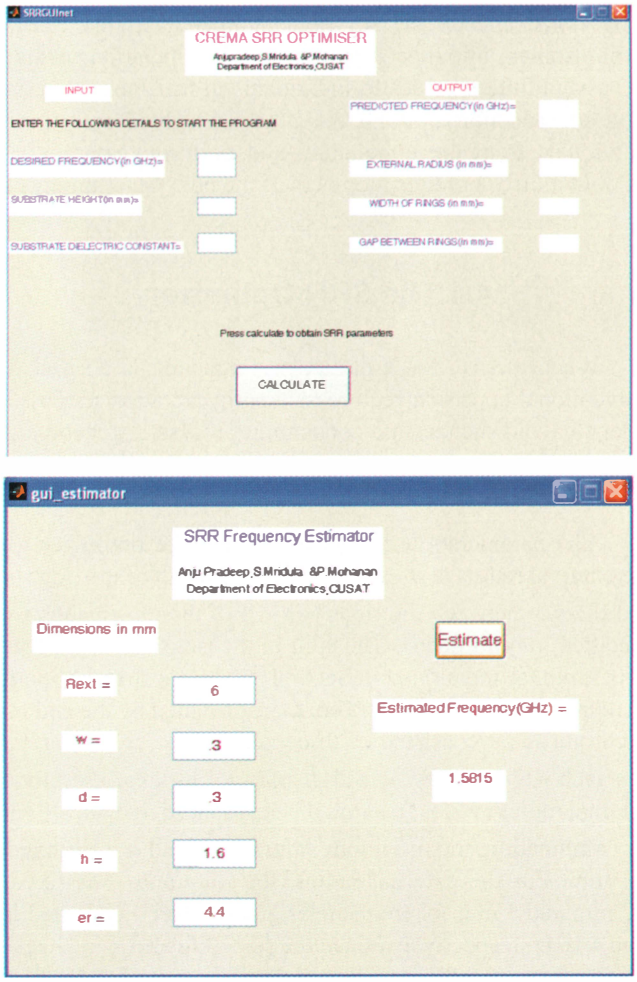

Figure 14. (a) The graphical user interface for the SRR optimizer; (b) the graphical user interface for the SRR estimator.

$0.2 \le (w,d) \le 1.7$, where $1.7 = [0.2 + (15 \times 0.1)]$;

$3 \le r_{ext} \le 9.3$, where $9.3 = [3 + (63 \times 0.1)]$, $f < 4$ GHz;

$1.7 \le r_{ext} \le 8.0$, where $8 = [1.7 + (63 \times 0.1)]$, $f > 4$ GHz.

The minimum inner radius of the inner ring was limited to 0.3 mm. 20 was chosen as the strength of the population. The cost function was the difference between the desired frequency and the predicted frequency:

$$\text{Cost} = \text{desired frequency} - \text{predicted frequency}.$$

The initial population was created randomly, and the resonant frequency corresponding to each chromosome was calculated. The resonant frequency thus obtained was used to compute the cost function. If the cost did not attain a minimum in the current population, individuals were selected from the lot for reproduction. A new generation was created through crossover and mutation, and iterations were continued until the cost attains a minimum. A simple flowchart of the developed optimizer is shown in Figure 13.

Validation of the optimizer was done for different desired frequencies. As expected, different design options were obtained for the same desired frequency, because of the various possible combinations. The results obtained were verified experimentally, and through simulation using Ansoft *HFSS*. Some results are tabulated in Table 1.

The current distribution was also studied to ascertain that the optimizer had chosen the first resonance. It was confirmed that the optimizer worked satisfactorily within a 10% error in the range of 1 GHz to 8 GHz. The graphical user interface for the SRR optimizer designed using *MATLAB* is shown in Figure 14a. The optimizer displays the SRR parameters for the required frequency. To calculate the resonant frequency of a given SRR, another graphical user interface was made, using the above equations. This estimator is shown in Figure 14b. This software can be freely downloaded from http://www.doe.cusat.edu/mohan.

5. Conclusions

Exhaustive experimental and simulation studies conducted on a ring-type split-ring resonator (SRR) to clearly understand the properties inherent in the SRR and the external factors affecting it were presented in this paper. It was observed that the resonant frequency was directly proportional to the width of the ring (w), the gap between rings (d), and the height of the substrate (h) (up to a height of 1.4 mm, after which the effect saturated). The resonant frequency was also inversely proportional to the radius of the SRR (r_{ext}) and the dielectric constant of the substrate. From studies on SRRs in different excitation environments, it was concluded that the resonant frequency was independent of the excitation, but its

Table.1 Verification of the results obtained through the optimizer, for a substrate height of $h = 1.6$ mm and a dielectric constant of $\varepsilon_r = 4.4$.

Desired Frequency (GHz)	SRR Parameters Obtained from GA Optimizer			Optimizer Predicted Frequency (GHz) (f_1)	Simulated Frequency (GHz) (f_2)	Experimental Frequency (GHz) (f_3)	% Error $100\left[(f_3 - f_1)/f_3\right]$
	r_{ext} (mm)	w (mm)	d (mm)				
1.2	8.6	0.9	0.2	1.201	1.27	1.15	4.3
2	6	0.5	0.7	1.98	1.94	1.97	0.5
2.8	5.7	1.7	1	2.743	2.88	2.7	1.48
3	4.8	1	1	2.874	3.1	2.91	1.37
4.2	3	0.3	0.9	4.23	4.3	4.22	0.23

polarizability strongly depended on the external fields impinging on the SRR. The negative-permeability effect was experimentally proven by inserting the SRR into a waveguide cavity.

The design equation was validated through experiment and simulation. This method can predict the resonant frequency with an error less than 10% for frequencies in the range of 1-8 GHz. User-friendly dedicated software was developed, using the genetic algorithm, for obtaining the dimensions of an SRR for a desired frequency. A front-end using *MATLAB* was developed for this purpose. The intriguing physical properties of metamaterials can be made use of in many important technological applications, such as the reduction of the radiation hazard in mobile phones, and the reduction of radar cross sections.

6. References

1. Christophe Caloz, "Perspectives on EM Metamaterials," *Materials Today*, **12**, March 2009, pp. 12-20.

2. Ricardo Marques, Francisco Medina and Rachid Rafii-El-Idrissi, "Role of Bianisotropy in Negative Permeability and Left-Handed Materials," *Physical Review B*, **65**, April 2002, pp. 144440 1-6.

3. B. Pendry, A. J. Holden, D. J. Robbins and W. J. Stewart, "Magnetism from Conductors and Enhanced Nonlinear Phenomena," *IEEE Transactions on Microwave Theory and Techniques*, **47**, 11, November 1999, pp. 2075-2084.

4. J. Garcia-Garcia, F. Martin, J. D. Beena, R. Marques and L. Jelinek, "On the Resonances and Polarizabilities of Split Ring Resonators," *Journal of Applied Physics*, **98**, August 2005, pp. 033103 1-9.

5. F. Bilotti, A. Toscano, L. Vegni, K. Aydin and K. Boratay, "Equivalent Circuit Models for the Design of Metamaterials Based on Artificial Magnetic Inclusions," *IEEE Transactions on Microwave Theory and Techniques*, **55**, 12, December 2007, pp. 2865-2873.

6. H. A. Bethe and J. Schwinger, "Perturbation Theory for Cavities," *NRDC Cornell University*, New York, March 1943, Report No. D1-117.

7. R. A. Waldron, "Perturbation Theory of Resonant Cavities," *Proceedings of the IEEE*, **107C**, September 1960, pp. 272-274.

8. Shuh-Han Chao, "Measurement of Microwave Conductivity and Dielectric Constant by the Cavity Perturbation Method and Their Errors," *IEEE Transactions on Microwave Theory and Techniques*, **33**, 6, June 1985, pp. 519-526.

9. Mi Lin, H. Duane Megan and M. N. Afsar, "Cavity Perturbation Measurement of Complex Permittivity and Permeability of Common Ferrimagnetics in Microwave Frequency Range," *IEEE Transactions on Magnetics*, **42**, 10, October 2006, pp. 2885-2887.

10. Ricardo Marques, Ferran Martin and Mario Sorolla, *Metamaterials with Negative Parameters – Theory, Design and Microwave Applications*, New York, John Wiley and Sons, 2007, Chapter 3, pp. 146-153.

11. Randy L. Haupt, "An Introduction to Genetic Algorithms for Electromagnetics," *IEEE Antennas and Propagation Magazine*, **37**, 2, April 1995, pp. 7-14.

12. J. Michael Johnson and Yahya Rahmat-Samii, "Genetic Algorithm Optimization and its Application to Antenna Design," IEEE International Symposium on Antennas and Propagation *Digest*, **1**, June 1994, pp. 326-329.

13. J. Michael Johnson and Yahya Rahmat-Samii, "Genetic Algorithms in Engineering Electromagnetics," *IEEE Antennas and Propagation Magazine*, **39**, 4, August 1997, pp. 7-21.

7. Acknowledgement

The authors gratefully acknowledge DST, UGC, and DRDO Government of India for financial support.

Introducing the Feature Article Authors

Anju Pradeep was born in India. She received the BTech degree in Electronics and Communication from Kerala University in 1993, and the MTech degree in Microwave and Radar Engineering in 2008 from Cochin University of Science and Technology (CUSAT). She is currently pursuing a PhD degree at CUSAT. She has been involved in teaching undergraduate students in engineering colleges since 1995. She was awarded the Young Scientist Award in the field of physical sciences for the best paper presentation at the first Kerala Women's' Science Congress 2010. Her areas of interest include metamaterials and optimization techniques. She is a life member of the Indian Society for Technical Education.

S. Mridula was born in India. She received the BTech degree in Electronics and Communication from the Kerala University in 1988, and the MTech degree in Electronics from the Cochin University of Science and Technology (CUSAT) in 1999. She was awarded the K. G. Nair Endowment Gold Medal for securing the first rank in the university. She received her PhD in Microwave Electronics from CUSAT in May, 2006. She has over 19 years of teaching experience in various professional institutions in Kerala, and is presently serving as Reader, Division of Electronics Engineering, School of Engineering, CUSAT. Her areas of interest include planar antennas, dielectric-resonator antennas, radiation hazards of mobile handset antennas, and computational electromagnetics. She is a member of the IEEE, a life member of the Institute of Electronics and Telecommunication Engineers (India), and a life member of the Indian Society for Technical Education.

P. Mohanan received the PhD degree in Microwave Antennas from Cochin University of Science and Technology (CUSAT), Cochin, India, in 1985. He worked as an Engineer in the Antenna Research and Development Laboratory, Bharat Electronics, Ghaziabad, India. Currently, he is a Professor in the Department of Electronics, CUSAT. He has published more than 130 refereed journal papers and numerous conference articles. He also holds several patents in the areas of antennas and material science. His research areas include microstrip antennas, uni-planar antennas, ultra-wideband antennas, dielectric-resonator antennas, superconducting microwave antennas, reduction of radar cross sections and polarization-agile antennas. Dr. Mohanan received the Career Award from the University Grants Commission in Engineering and Technology, government of India, in 1994.